Supplementary Information

A. Major sites along the inland traverse.

Table A. Major sites along the inland traverse.

Site Name	Lat ◦ S	Long ◦ [a]	Elevation	H [b] (m)	Legs [c]	Notes
S16	69.030	40.052	589	350	CE	Base of the Japanese team near the coast
Mizuho	70.697	44.274	2250	2060	CE	
MD170	72.273	43.728	2749	2335	CE, ME	
MD384	74.185	42.886	3381	2381	P9, ME	
MD585	75.983	41.194	3679	2078	P1, P9	
DF	77.317	39.703	3800	3028	P1, P3, P4, P5	Dome Fuji Station. Site of 3035 m long borehole
SSW47	77.801	39.040	3761	2157	P3	Site above subglacial mountains
SSW90	78.164	38.538	3709	2661	P3	Site above high-shearing above subglacial mountains
SSW150	78.683	37.795	3656	3124	P3	Southernmost point of the survey in 1996/1997 season
DF80	77.373	39.617	3798	2790	P2, P3	End point of leg P2
East95	77.363	43.568	3714	3027	P2	Subglacial Lake Point, Lake ID [d] 97
East130	77.361	45.01	3669	2274	P2	Easternmost point of the survey in 1996/1997 season
RT441	77.498	37.428	3770	3154	P4	Subglacial Lake Point, Lake ID 89
RT313	77.961	32.624	3620	3249	P4, P6	Subglacial Lake Point, Lake ID 93
RT188	77.161	29.426	3678	2473	P6	Profile corner
RT155	76.869	29.270	3701	2601	P6	Profile corner
MP	75.888	25.834	3661	2792	P5, P6, P7, P8	Meeting point of the two national teams
NCR62	75.428	27.153	3589	2772	P7	Northernmost point of the cross-ridge traverse at the meeting point
A38	75.287	18.421	3543	2706	P8	
A28	74.862	14.742	3466	–	P8, MW1	End point of leg P8
EPICA DML	75.004	−0.006	2890	2774	MW1, MW2	Site of 2774 m-long borehole
IPY Site1	75.001	−10.121	2528	1603	MW2, CW	Science stopping point
–	74.454	−11.572	1078	1689	CW	Southern side of the Veststraumen Ice Stream
–	74.046	−12.006	998	1591	CW	Northern side of the Veststraumen Ice Stream
Wasa Station	73.053	−13.374	292	383	CW	Base of the Swedish Team

[a] Positive and negative longitudes indicate east and west, respectively.
[b] H : ice thickness (m).
[c] Legs including the site.
[d] Lake ID is from Popov and Masolov (2007).

B. Comparison between radar diagnosis of the bed with data of ice motion in Antarctica

The diagnosed bed conditions are compared with a digital mosaic of ice motion in Antarctica assembled from satellite interferometric synthetic-aperture radar data (InSAR) compiled by Rigout et al. (2011a, 2011b), because fast motion of the ice is frequently associated with large basal motion. A preliminary comparison between ice deformation velocity and InSAR velocity shows that most of the observed motion in Shirase Glacier is caused by basal movement (Fig. 2D in Rignot et al., 2011a). In the Shirase glacier basin, we found a temperate bed, which is consistent with the argument by Rignot et al. that surface motion is a result of large basal motion in this area.

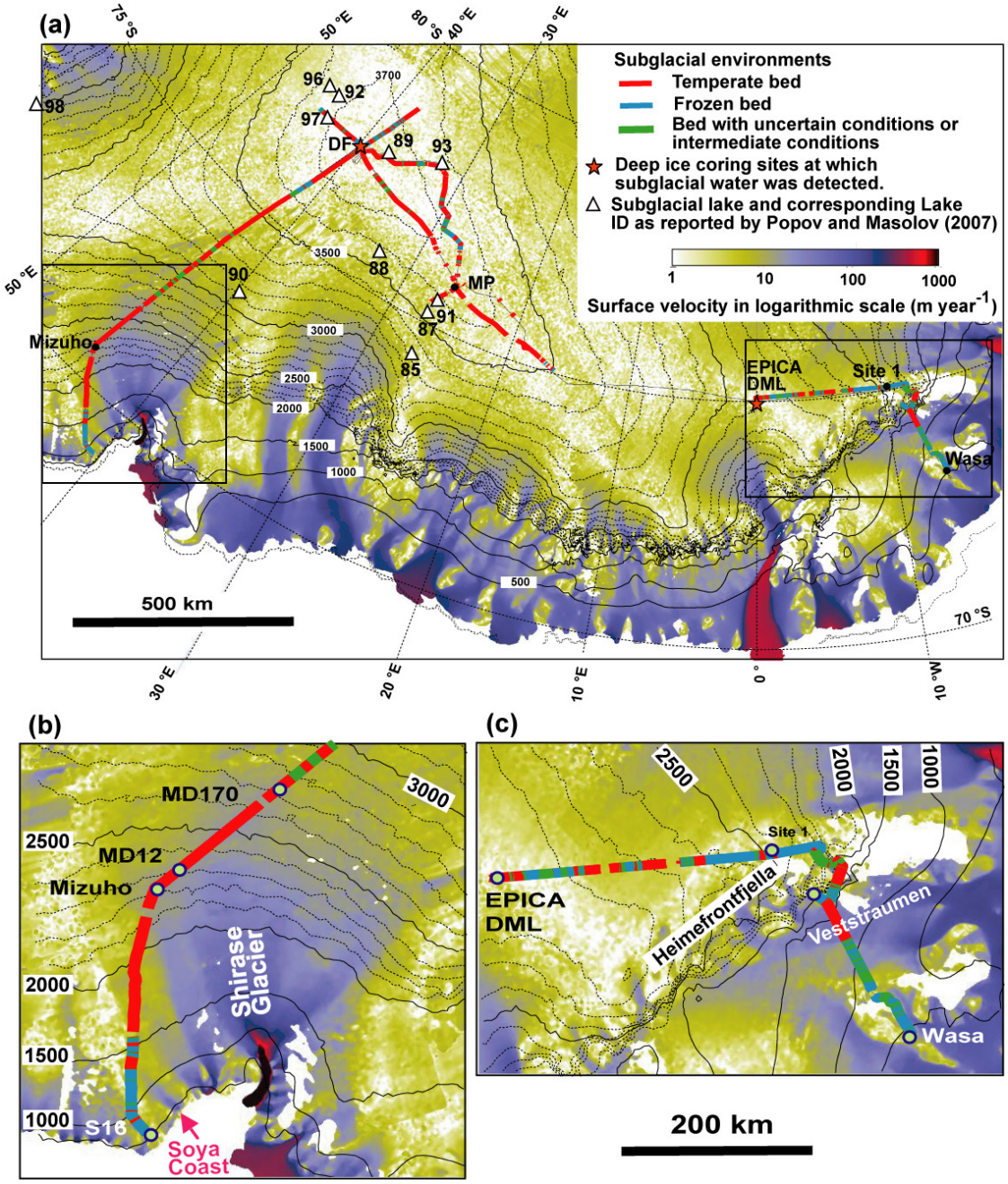

Fig. B. Predicted bed conditions are shown on ice velocity map of DML (Rignot et al., 2011a, 2011b). The overlying red, blue and green dots indicate sites that we diagnosed as temperate, frozen, and unceratain/intermediate, respectively. The colour scale of ice flow velocity is in logarithmic scale. Surface elevation is shown by thin black contours. The other symbol markers

and elevation contour lines are the same as in Fig. 1 in the main text. (b, c) details of two areas close to fast-flowing glaciers.

References

Rignot, E., Mouginot, J., and Scheuchl, B.: Ice flow of the antarctic ice sheet, Science, 333, 1427-1430, 10.1126/science.1208336, 2011a.

Rignot, E., Mouginot, J., and Scheuchl, B.: MEaSUREs InSAR-Based Antarctica Velocity Map. Boulder, Colorado USA: NASA EOSDIS Distributed Active Archive Center at NSIDC. Accessed on June 12, 2012. http://nsidc.org/data/nsidc-0484.html, 2011b.

C. Modelling two-way attenuation

Fig. C shows the depth-averaged, one-way attenuation rates <*N*> estimated with the model. As ice thickness increases, <*N*> increases where the bed is frozen, while <*N*> decreases when the bed is temperate. In the radar data analysis, linear least-squares fit was made for $[P^{c}_{\mathrm{bed}}]_{\mathrm{dB}}$ over the ice thickness range between 1700 m and 2600 m for the P legs. For the model results in this ice thickness range, the ensemble-mean <*N*> is 4.5 dB km^{-1}.

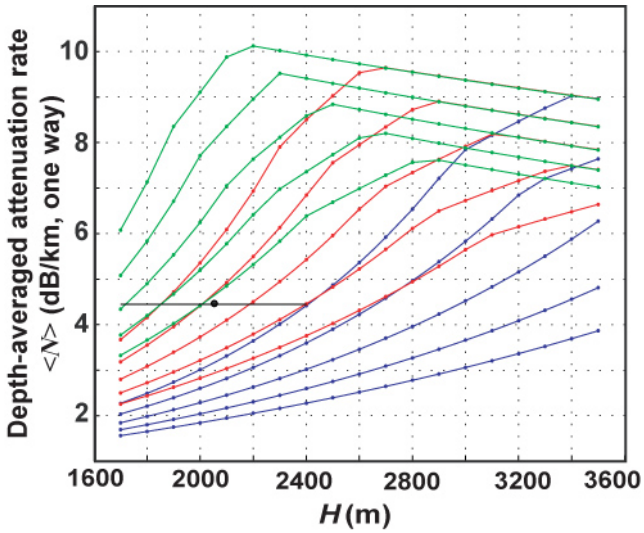

Fig. C. Depth-averaged attenuation rates. Green, red, and blue curves show the cases for geothermal fluxes of 40, 50, and 60 mW m^{-2}. For each geothermal flux, five curves show the cases for surface mass balance (ice equivalent) of 20 mm yr^{-1} (top), 30 mm yr^{-1}, 40 mm yr^{-1}, 50 mm yr^{-1}, and 60 mm yr^{-1} (bottom). The black dot shows the ensemble-mean <*N*> for the ice thickness between 1700 m and 2400 m, which is equivalent to the handle of the hockey stick found for the P legs.

D. Overview of the approach to diagnose the subglacial conditions

Overview of the approach to daignose the subglacial conditions

STEP 1: H-P Plot diagnosis

Possible conditions and related empirical features of data are as follows.

Only frozen conditions exist within a data set covering an area.	Frozen and temperate conditions co-exist within a data set covering an area.	Only temperate conditions exist within a data set covering an area.
• $[P^c_{bed}]_{dB}$ tends to decrease with increasing H. • Tracks of the data points tends to follow this tendency.	• $[P^c_{bed}]_{dB}$ decreases with increasing H. However, anomalous increases of $[P^c_{bed}]_{dB}$ appear at large H value. As a result, large scale distribution of the data has a shape of hockey stick. • Points for the anomalous increases are likely to be frozen/temperate boundaries. However, H for the frozen/temperate boundary are variable from one location to another. • At temperate beds, tracks of the data points tend to have fluctuation both in near vertical directions and near horizontal directions, presumably due to heterongeneously distributed water at the bed.	• $[P^c_{bed}]_{dB}$ decreases with increasing H. However, this correlation can be highly obscured or erased by heterongeneously distributed water at the bed. No hockey stick like features are found. • At temperate beds, tracks of the data points tend to have fluctuation both in near vertical directions and near horizontal directions, presumably due to heterongeneously distributed water at the bed.

STEP 2: X-HP plot diagnosis and δP plot diagnosis

Possible conditions and related empirical features of data are as follows.

Only frozen conditions exists within a data set covering an area.	Frozen and temperate conditions co-exist within a data set covering an area.	Only temperate conditions exist within a data set covering an area.
• Profiles of $[P^c_{bed}]_{dB}$ and H tend to agree in the X-HP plot.	• At temperate bed, profiles of $[P^c_{bed}]_{dB}$ tend to be larger than those of H in the X-HP plot. • As a result, $\delta[P^c_{bed}]_{dB}$ of temperate bed tend by higher than those of frozen bed in the δP plot by 10-20 dB. However, $\delta[P^c_{bed}]_{dB}$ does not provide solid numerical criteria for the temperate/frozen delineation because of variability of the attenuation.	• Profiles of $[P^c_{bed}]_{dB}$ and H tend to have weak correlation. However, this correlation can be highly obscured or eliminated by heterongeneously distributed water at the bed. • In some cases, $[P^c_{bed}]_{dB}$ exhibits large fluctuations and sharp peaks with widths of from 1 km to several km, presumably due to heterongeneously distributed water at the bed.

STEP 3: Crosschecking and collection of additional information

If the diagnosis procedures above do not provide convincing results, this step is important.

(i) Compare the results of diagnosis between neighboring areas.
If only temperate conditions exist within a data set covering an area, $[P^c_{bed}]_{dB}$ can be higher by 10-15 dB than $[P^c_{bed}]_{dB}$ of neighbouring frozen bed.
(ii) Check the elevation of the ice sheet surface and the range of H to determine whether the results of diagnosis appear to be reasonable.

Fig. D. Overview of the approach to diagnose the subglacial conditions using the H-P plot, the X-PH plot, the X-δP plot, and other information.

E. Examination of the Raymond Effect

In the main text of this paper, we suggested that the Raymond effect underneath divides explains why temperate ice could appear at the bed where thickness *H* of ice is considerably smaller than ~2800 m. This seems somewhat contradictory, as the Raymond effect is less pronounced when the bed is not rigid. Martin et al. (2009) showed that sliding can damp or eliminate the operation of the Raymond effect under certain conditions. If the Raymond effect is strong enough to change the temperature field at the bed, then it should also be found in isochrone arches (Raymond bumps), which are best seen in radar data perpendicular to the ice divide. Clarification of this issue using radar isochrone data is useful and informative. In addition, numerical modelling should also be useful to assess whether the Raymond effect can make an anomalous thermal regime at the bed.

(i) Assessment of dynamical conditions along the ridge using numerical models

Seddik (2008) and Seddik et al. (2011) modelled ice flow in a 200×200 km domain around the Dome Fuji drill site that includes DF and MP. They used a three-dimensional thermo-mechanically coupled ice-flow model that accounts for anisotropy of ice rheology associated with alignments of ice crystals. Steady-state simulations for the present-day conditions shows that basal temperature is at the pressure melting point below the ridge between DF and MP whereas the bed temperature is below the pressure melting point by several degrees at sites roughly 20 km or more further from the current divide locations (see Fig. 10 in Seddik et al., 2011).

(ii) Appearance of the Raymond effect in the morphology of the isochrones

Shape of isochrones along legs P1-P3 and P7 are shown in Fig. E. They lie across the ridge at Dome Fuji and MP. Data at legs P1-P3 are partly shown in Fig. 13 in the TCD version of the present paper. Along these cross-ridge legs, depths of the isochrones vary by several hundred metres, which are correlated with the bed elevation changes. However, the deep isochrones show anomalous features near Dome Fuji: there is an upward arch over a horizontal distance of several tens of kilometres. The bed underneath this feature is a trough, so the shape of this isochrone is not directly related to the bed topography. We speculate that this is a feature of the local effect at the ice divide known as the Raymond effect. Martin et al. (2009) discussed that strength and spatial distribution of the effect depending on the strength of flank flows, migration history of the ice divide, basal sliding, and so on. In addition, complex bedrock topography with heterogeneous distribution of temperate/frozen conditions may add further complications. Discussions for these factors will be complex, and seem beyond the scope of the present paper. As for the 40 km-long leg across the ridge at MP, we cannot identify such an anomalous shape of the isochrones. This may be caused because the glaciological conditions are different between DF and MP or because the radar profile at MP is much shorter than that at DF, so such a feature is hard to identify.

References

Martin, C., Hindmarsh, R. C. A., and Navarro, F. J.: On the effects of divide migration, along-ridge flow, and basal sliding on isochrones near an ice divide, Journal of Geophysical Research-Earth Surface, 114, 17, F02006 doi:10.1029/2008jf001025, 2009.

Seddik, H. (2008). "A full-Stokes finite-element model for the vicinity of Dome Fuji with flow-induced ice anisotropy and fabric evolution." Doctoral thesis, Graduate School of Environmental Science, Hokkaido University, Sapporo, Japan. Hokkaido University Collection of Scholarly and Academic Papers (HUSCAP).

Seddik, H., R. Greve, et al. (2011). "A full Stokes ice flow model for the vicinity of Dome Fuji, Antarctica, with induced anisotropy and fabric evolution." The Cryosphere 5: 495-508.

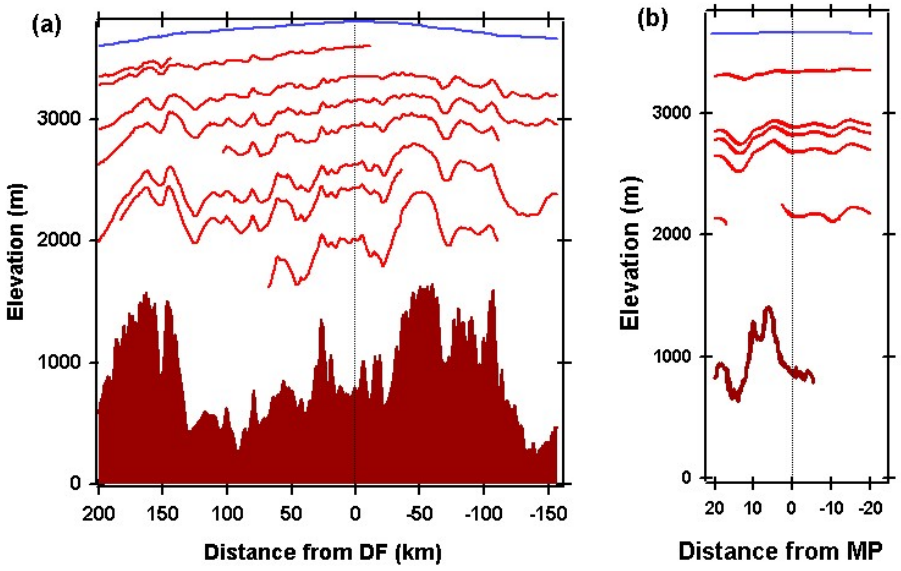

Fig. E. Distribution of major isochrones for (a) legs P1 and P3 and (b) ridge at MP. (a) Distance from Dome Fuji is measured towards the south-southwest. The ordinate is elevation above the WGS84 ellipsoid. The uppermost blue trace is the surface of the ice sheet. Red traces are isochrones extracted from radar images. Shaded area in brown is the bed. (b) Distance is measured from site MP towards the south-southwest.

F. Comparison between radar-based and model-based assessments of the bed conditions

In Section 4.3, we discussed our results of bed diagnosis in the context of model-based assessments (Pattyn, 2010). Our radar results show that at least 56% of the bed profiled in this study is temperate, and at least 14% is frozen. This fraction is similar to the model-based diagnosis, which gives 55% of the bed over all of the Antarctic ice sheet as temperate and 45% as frozen. In this supplemental discussion, we further compare these results.

The background image in Fig. F shows the model-predicted ensemble-mean basal melting rate. Overlaying profiles show our diagnosis of the bed condition. Overall, the model prediction agrees well with our radar data interpretations. As we discussed in the main text of the paper, beds of the inland part of the ice sheet tend to be temperate, with the exception of subglacial high mountains. In contrast, beds of coastal areas tend to be frozen, with the exception of fast-flowing ice in subglacial lowlands or troughs. These conditions are found both in our observation and in the model of Pattyn (2010). We found that the bed is continuously temperate inland of Mizuho in which a tributary of Shirase Glacier penetrates. However, Pattyn's model predicted large variations of the basal melting rate between <0.2 mm a^{-1} (insignificant, white in the figure) and several millimetres per year. We argue that this discrepancy can be explained if the local melt rate is small but subglacial water flows into this area from the large drainage basin, which is also inferred by Pattyn's model (see his Figure 5).

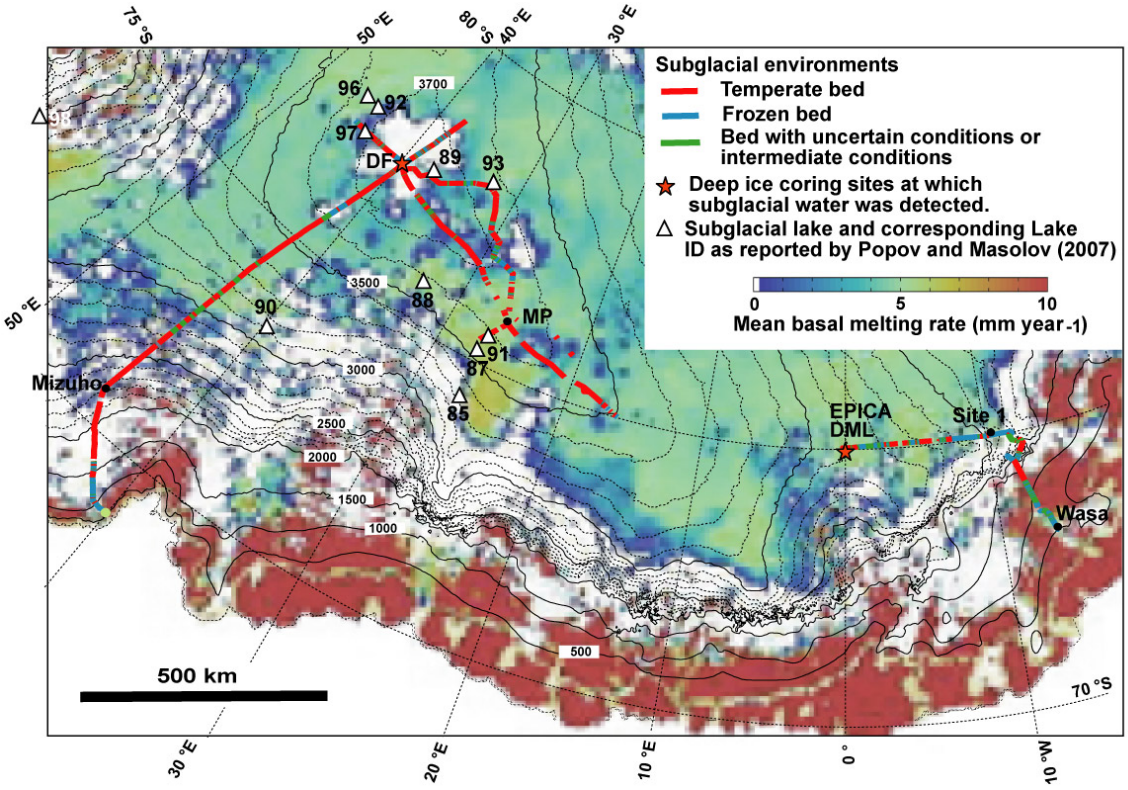

Fig. F. Model-predicted basal melting rate (Pattyn, 2010) together with radar diagnosis of the frozen and temperate beds. The background image was reprinted from Figure 4A in Pattyn (2010), Copyright (2010), with permission from Elsevier.

Reference

Pattyn, F.: Antarctic subglacial conditions inferred from a hybrid ice sheet/ice stream model, Earth

Planet. Sc. Lett., 295, 451–461, doi:10.1016/j.epsl.2010.04.025, 2010.